



How Lasers Exploit Photoacoustic and Photoelectric Phenomena to Inject Signals into MEMS Microphones

Benjamin Cyr¹ · Vedant Sumaria² · Yan Long¹ · Srinivas Tadigadapa² · Takeshi Sugawara³ · Kevin Fu²

Received: 1 April 2024 / Accepted: 6 February 2025
© The Author(s) 2025

Abstract

An amplitude-modulated laser can be used to generate false, yet coherent acoustic signals on the outputs of MEMS microphones. While this vulnerability has ramifications on the security of cyber-physical systems that trust these microphones, the physical explanation of this effect remained a mystery. Without an understanding of the physical phenomena contributing to this signal injection, it is difficult to design effective and reliable defenses. In this work, we show the degree to which the mechanisms of thermoelastic bending, thermal diffusion, and photocurrent generation are used to inject signals into MEMS microphones. We provide models for each of these mechanisms, develop a procedure to empirically determine their relative contributions, and highlight the effects on eight commercial MEMS microphones. We accomplish this with a precise setup to isolate each mechanism using several laser wavelengths and a vacuum chamber. The results indicate that the injected signal on the microphone is dependent on the wavelength of the incoming light. Shorter wavelengths (such as a 450 nm blue laser) exploit photoacoustic effects, and the periodic heating and expansion of air is the dominant factor in seven of eight sample microphones. Longer wavelengths (such as a 904 nm infrared laser) exploit photoelectric effects on the sensitive ASIC, generating signals that are between 2x and 100x stronger than photoacoustic signals in six of eight sample microphones. This understanding of the physical causality of laser signal injection leads to recommendations for future laser-resistant microphone designs. These include adding light-blocking structures at the system or device level, improving to glob top application, and adding simple light or temperature sensors for injection detection. Based on the fundamental causality, we also suggest potential vulnerabilities within other sensors with similar characteristics to MEMS microphones, such as conventional microphones, ultrasonic sensors, and inertial sensors.

Keywords Lasers · MEMS · Sensors · Photoacoustics · Injection attacks

1 Introduction

Our previous research *Light Commands* [1] demonstrated how maliciously false and coherent acoustic signals can be induced by firing a laser beam into the acoustic port of a MEMS microphone (Fig. 1). This effect demonstrated a new vulnerability that allows an adversary to achieve control over devices such as IoT voice assistants by delivering stealthy audio commands. The crafted light signal generates a voltage signal on the output of the microphone, which is blindly interpreted as an acoustic signal by the downstream systems. In such conditions, *Light Commands* can inject any voice commands into a system that takes input from MEMS microphones. The research also showed the ease of using milliwatt amplitude-modulated lasers to induce false acoustic emanations

into MEMS microphones behind glass windows and over 100m away. This significantly expanded the attack surface of smart home devices, allowing a malicious attacker to use a laser to potentially unlock smart locks, open garage doors, start vehicles, make online purchases, or control smart home appliances. As a result, the *Light Commands* vulnerability in MEMS microphones used in smart devices today could pose threats to not only the security and financial assets but also the safety of IoT, mobile, and emerging smart device users.

This was a surprising result within the security and privacy community, reshaping the perspectives on threat models for devices that rely on voice commands or other acoustic information to perform automated tasks. While this previous work investigated and presented the security risks of current systems reliant on MEMS microphones, there was only an initial investigation into the causality of this laser

Extended author information available on the last page of the article

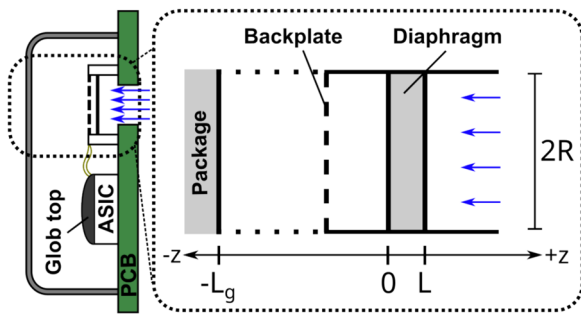


Fig. 1 The coordinate system used for the MEMS microphone model. Light enters the acoustic port, interacting with the MEMS structure and the ASIC

signal injection phenomenon. Given that this research had major security implications for microphone-reliant devices and has generated many follow-up security exploitation and mitigation efforts [2–7], it is crucial to further model the physics-based principles for why the injection succeeded as a contribution to both science and secure hardware manufacturing.

In this work, we perform an in-depth investigation of the causality of *Light Commands*, identifying each of the potential physical effects that can generate false acoustic signals, and provide a procedure by which hardware designers can use to determine the effects that are making their microphones vulnerable to laser signal injection attacks. To properly design security defenses for light-resistant microphones, one must first understand the underlying physics-based causality of the *Light Commands* vulnerability. Thus, our discoveries enable defenses that are more deliberate and with measurable tolerance to *Light Commands* attacks.

We make the following contributions:

- We develop a model of laser signal injection into MEMS microphones consisting of three physical mechanisms: thermoelastic bending, thermal diffusion, and photocurrent generation (Sect. 3).
- We describe and perform an experimental procedure to isolate the contributions of each of the effects on a set of eight commercial microphones, highlighting the specific physical vulnerabilities within each microphone to laser signal injection (Sect. 4).
- Using this model and experimental results, we recommend design changes to decrease the sensitivity of MEMS microphones to light signal injection and indicate other sensors that may be vulnerable (Sect. 5).

2 Background

Previous laser attacks on sensitive electronics exploited photoelectric effects to control the output of a system. This

includes laser fault injection attacks [8, 9], where light is used to cause bit-flips and errors in digital computing devices to bypass security mechanisms. In particular, these works use photoelectric effects to generate a current across photosensitive transistors and other p-n junctions built into the semiconductor chips. This even allows analog control over some circuits, such as the analog control of clock timing as demonstrated in RedShift [10]. Because photoelectric mechanisms are also used in sensors designed to sense light, it was also exploited in previous laser signal injection attacks on infrared drip sensors [11], LiDAR [12], and cameras [13, 14].

Because of these previous works, it was natural to simply assume that photoelectric effects were to blame for the laser signal injection in MEMS microphones. MEMS microphones come in many different designs, but they all function by measuring the motion of a thin diaphragm as it responds to fluctuations in air pressure. Because of the small scales and environmental sensitivity of MEMS devices, amplification and measurement circuits are required to remove noise and generate an output signal approximately proportional to the displacement of the diaphragm [15]. These circuits are designed into an application specific integrated circuit (ASIC) that is packaged adjacent to the MEMS structure (see Fig. 1). While often protected from environmental effects via an opaque epoxy or “glob top,” it was hypothesized that *Light Commands* was exploiting photoelectric effects as light entered the microphone package and struck the sensitive amplifying and measurement circuits on the ASIC.

But our in-depth research in *Light Commands* causality also suggested the possibility of exploiting photoacoustic effects in MEMS microphones. Photoacoustics is the study of the generation of vibrations in response to incoming light, and it has been studied extensively for its applications in materials science and biomedical sensing [16]. There are many thermomechanical and electromechanical processes that have been investigated [17–20], but only a few works have investigated the consequences on MEMS structures. For example, Todorović [21] and several follow-up works by related researchers [22–24] investigated photoacoustic effects on silicon microstructures, noting several potential effects. Strahl et al. [25] actually used a MEMS microphone as a photoacoustic cell to detect methane, demonstrating future photoacoustic sensing capabilities with these devices.

2.1 Characterizing MEMS Microphone Response to Lasers

The *Light Commands* vulnerability reveals an emerging research need for understanding how MEMS microphones behave when excited by laser stimuli. While only a few prior works have investigated this phenomenon and presented rudimentary hypotheses, this work presents the first experimental

characterization and systematic modeling of the physical process. Below, we introduce how this work advances this emerging research field compared to a few prior works.

Besides the original *Light Commands* paper [1] which verifies lasers can generate acoustic signals on MEMS microphones outputs for the first time, our follow-up work [26] provides preliminary experimental evidence that photoacoustic effects on the diaphragm were the primary contributor to the laser injection signal. Building on this, a recent work [27] designed several experiments that confirmed the significant impact of photoacoustic effects in *Light Commands* attacks. Furthermore, they introduced the concept of L-shaped sound path attacks, demonstrating that even reflected laser-induced light can trigger MEMS microphone outputs in mobile phones. While [27] advanced the understanding of this attack, it still leaves room for a comprehensive model that accounts for how different effects besides photoacoustic effects can affect MEMS microphones under different wavelengths. As we will demonstrate in this work, photoelectric and other effects could play a more important role in certain conditions.

Since such a model and understanding is a key part to developing future MEMS microphones that are resistant to laser signal injection, our work continues from this previous research to provide the first experiment-based physical description of the laser signal injection into MEMS microphones. Specifically, this work performs several experiments to determine that the output of the microphones is caused by a linear combination of three photoacoustic and photoelectric

effects. We describe each of these effects and show how they contribute towards the generation of an output voltage signal that is dependent on the design of the MEMS microphone. In addition, we present our experiments as a procedure to be used by MEMS microphone designers to determine which effects are applicable to their microphones. We present this procedure so that progress can be made with future designs to reduce the vulnerability of MEMS microphones to laser signal injection.

3 A Model of Laser Signal Injection in MEMS Microphones

We begin by presenting a model of the laser signal injection and the effects that generate the output signal on the MEMS microphone. The effects of laser signal injection into MEMS microphones can be described by the combination of three different physical mechanisms (Fig. 2):

- Thermoelastic (TE) bending [19, 24]: As the MEMS structures absorb the incoming light, they heat up and expand. This displaces the diaphragm when a bending moment is generated by thermal asymmetries within the diaphragm.
- Thermal diffusion (TD) [17, 18]: As the diaphragm heats up, it also heats the surrounding air. The periodically heated air column expands adiabatically, generating a pressure wave that displaces the diaphragm.

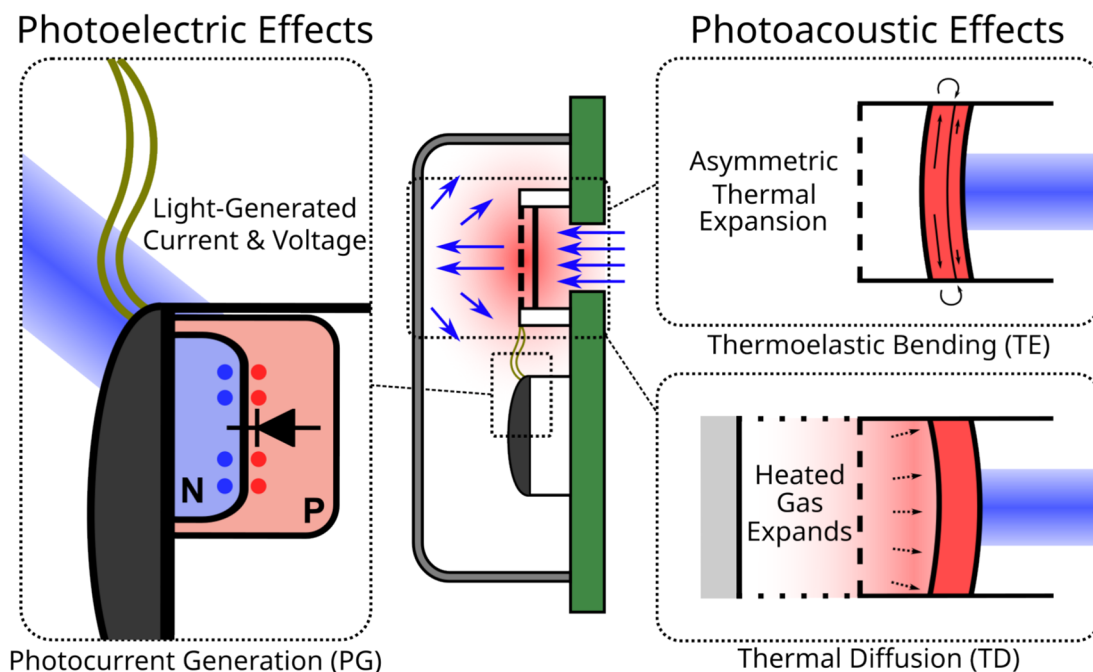


Fig. 2 A summary of the three primary physical phenomena that were investigated in this work. Two mechanisms are photoacoustic and dependent on the heating of the diaphragm and the air. The last one is photoelectric and dependent on carrier generation within the ASIC

- Photocurrent generation (PG) [28]: As light interacts with semiconductor components, it generates excess charge carriers. When these charge carriers appear within p-n junctions on the ASIC, it will generate a photocurrent and voltage signal that will be coupled to the output voltage of the microphone.

There are several other physical mechanisms that can potentially cause effects on MEMS microphones, including thermal expansion [18, 21], plasmaelastic bending and contraction via charge-carrier generation [24, 29], and radiation pressure. While these other mechanisms can potentially contribute to a signal on the output of the microphone, they were disregarded due to low expected amplitudes within the context of this study. First, the diaphragms of the microphones are at thicknesses on the order of a micron, and the expansion and contraction coefficients are small, greatly reducing any expansion and contraction of the diaphragm thickness. Next, the thin, heavily doped diaphragms also allow charge carriers to diffuse and recombine quickly, reducing plasmaelastic effects. Finally, the expected magnitude of radiation pressure at the irradiances explored in this study are lower than the noise floor of the microphone. More thorough analyses of these other mechanisms are presented in Appendix A.

Because of the factors reducing other physical effects, we focused on the contributions of the three mechanisms of thermoelastic bending, thermal diffusion, and photocurrent generation. The models of these mechanisms rely on a coordinate system defined in Fig. 1. These effects are summarized in Fig. 2. Note that all physical parameters within these models are described by the real parts of any complex expressions.

3.1 Optical Irradiance Model

In the Light Commands attack, the optical power P of the attacking laser was modulated to inject an audio signal. By modulating the light, the result was a change in light irradiance (optical power density) entering the acoustic port of the microphone. Without any changes to aiming or focus, a single frequency component ω of the irradiance signal entering the acoustic port can be modeled as the real part of the complex expression:

$$I = I_B + I_0 e^{j\omega t} = [P_B + P_0 e^{j\omega t}] / A_B \quad (1)$$

where P_0 is the amplitude of the sinusoidal power signal entering the acoustic port, P_B is the bias on the optical power signal, and A_B is the cross-sectional area of the laser beam that enters the acoustic port (A_B will be equal to the cross-sectional area of the acoustic port in most attack cases). Since the irradiance cannot be less than zero, the amplitude I_0 must be less than I_B . Besides this condition, however, the contri-

bution of the bias signal I_B can often be ignored. Therefore, for the rest of this section, we will only consider the time-varying portion of this signal: $I_0 e^{j\omega t}$.

Assuming the angle of incidence is normal to the diaphragm, the MEMS diaphragm will reflect (I_R), transmit (I_T), and absorb (I_A) a certain amount of incoming irradiance depending on the wavelength λ of the incoming light:

$$I_R = R_\lambda I_0 e^{j\omega t} \quad (2)$$

$$I_T = T_\lambda I_0 e^{j\omega t} \quad (3)$$

$$I_A = [1 - R_\lambda - T_\lambda] I_0 e^{j\omega t} \quad (4)$$

where (R_λ) and (T_λ) are the optical reflectance and transmittance dependent on the light wavelength λ .

The amount of light that is reflected, transmitted, and absorbed is highly dependent on the materials and structure of the MEMS device and can quickly become difficult to model at a high optical transmittance (T_λ). In general, for the materials used in MEMS structures (such as polysilicon or aluminum nitride), the transmittance decreases as the wavelength of the incoming light decreases [30–32]. This means that shorter wavelength (“bluer”) light will be absorbed and blocked more than longer wavelength (“redder”) light. This is vitally important for understanding the contributions towards each of the physical effects on the microphones.

3.2 Thermoelastic Bending (TE)

The thermoelastic bending component of the photoacoustic signal results from thermal moments that are generated as the diaphragm is heated by the incoming laser signal. This effect was first modeled by Rousset et al. [19] from thermal moments arising from an asymmetric heat distribution through the thickness of a heated plate. In the case of MEMS diaphragms, however, the structures are thin and insulated by air, which has a relatively low thermal conductivity. This means that the heat diffuses through the thickness almost immediately, causing the diaphragm to be at a nearly uniform temperature. The temperature of the diaphragm (T_d) can be modeled by

$$T_d \approx \frac{I_A}{j\omega\rho c_p L} \quad (5)$$

where ρ is the density of the diaphragm material, c_p is the specific heat capacity, and L is the thickness of the diaphragm. Note that the temperature decreases as the frequency of modulation ω increases.

While Rousset’s model does not predict bending when there is a uniform temperature, there are still cases where bending can occur. Rather than an asymmetry of temperature, Todorović et al. [24] described the effects of an asymmetry of material properties between a substrate and a thin film.

The differences in elasticity shift the neutral plane (z_n), and the differences in thermal expansion generate a moment even in the case of uniform temperature. Using this model, a quasistatic analysis can represent the average displacement of the membrane with

$$w_{TE} = \frac{1}{4} R^2 M_T T_d \tag{6}$$

where R is the radius of the diaphragm, and M_T is a moment-generating constant determined from the thermal properties of the materials and geometry of the diaphragm:

$$M_T = \frac{\int_0^L \alpha_T(z) E(z-z_n) dz}{\int_0^L E(z)(z-z_n)^2 dz} \tag{7}$$

$$z_n = \frac{\int_0^L E(z) z dz}{\int_0^L E(z) dz} \tag{8}$$

where $\alpha_T(z)$ and $E(z)$ are the linear thermal expansion coefficient and Young’s modulus of the material at each coordinate through the diaphragm thickness L .

The important factors to consider for TE are the static material properties of the diaphragm, the frequency of the incoming modulation, and the light that is absorbed by the diaphragm. Shorter wavelengths will be absorbed more strongly by the diaphragm, but any absorbed light will generate a bending effect. Since the diaphragm temperature T_d is inversely proportional to the modulation frequency, the TE component will decrease by a factor of ω^{-1} as the modulation frequency increases.

3.3 Thermal Diffusion (TD)

Thermal diffusion or the “thermal-piston” effect is the process by which an acoustic pressure wave is generated as the air in the microphone periodically heats and expands. This effect was first described by Rosencwaig and Gersho [17] while performing photoacoustic experiments on a closed cell of air. In their model, an incoming laser signal is absorbed by a surface, causing a sudden increase in temperature. This heat then diffuses into the surrounding air. Because the air has a much lower thermal diffusivity than the absorbing surface, the heat conducts slowly, resulting in a layer of hot air close to the surface. This layer of air will expand adiabatically pushing out against the rest of the air within the closed cell and generating a pressure signal.

In the context of MEMS microphones, a pressure signal will be generated within the package and push the diaphragm outward. To determine the displacement of the microphone, we start by first modeling the average temperature of the gas column that extends from the MEMS structure to the back package. The average temperature of the air column can be calculated as described in [18] using a one-dimensional heat transfer model and using the temperature of the diaphragm

and the ambient temperature as the boundary conditions. The spatially averaged gas temperature reduces to

$$T_g = \frac{\tanh(L_g \sigma_g / 2)}{L_g \sigma_g} T_d \tag{9}$$

$$\sigma_g = \sqrt{j \omega / \alpha_g} \tag{10}$$

where L_g is the height of the gas column (the distance from the MEMS structure to the package), and σ_g is the complex thermal diffusion parameter defined from the modulation frequency ω and the thermal diffusivity of the air α_g .

Using the average temperature of the air column, the pressure signal can then be calculated from the ideal gas law with adiabatic expansion:

$$P = \frac{\gamma P_0 V_g}{V_0 T_0} T_g \tag{11}$$

$$V_g = \pi R^2 L_g \tag{12}$$

where P_0 , V_0 , and T_0 are the ambient pressure, volume of the microphone’s back cavity, and ambient temperature, respectively. The constant γ is the ratio of specific heats of air at constant pressure and constant volume, which can be approximated as 7/5. The volume of the heated air V_g is defined from the area of the MEMS structure and the height of the heated air column L_g .

From this pressure, the quasistatic average displacement of the diaphragm at low frequencies can be described with

$$w_{TD} = \frac{A_r \pi R^2}{K_d} P \tag{13}$$

where K_d is the effective spring constant of the diaphragm and A_r is the effective acoustic area coefficient, which accounts for the differences in displacement and pressure at each point on the diaphragm. The coefficient A_r is a number from 0 to 1, and it is dependent on the mechanical boundary conditions of the diaphragm. The mechanical model of the diaphragm has been explored in [33] and [34].

The TD component is primarily dependent on the temperature of the diaphragm and the acoustic properties of the microphone system. Notice that for low modulation frequencies, the heat diffuses entirely through the gas column. The average temperature can then be approximated as $T_g = T_d/2$, and the signal decreases at a rate of ω^{-1} . As the modulation frequency increases, however, the heat only diffuses part-way through the column, reducing the average temperature to $T_g = T_d / l_g \sigma_g$. In this case, the TD signal is proportional to $\omega^{-3/2}$, as σ_g is proportional to $\omega^{1/2}$. Therefore, the TD signal gets much weaker as the modulation frequency increases. Beyond the modulation frequency, the output signal will be directly proportional to the ambient pressure. This can be used to isolate the TD phenomenon, as it is the only one to be primarily affected by changes to this ambient condition.

3.4 Photocurrent Generation (PG)

The laser will affect the output voltage of the microphone by inducing a photocurrent within the signal measurement and processing circuits on the ASIC. The photocurrent generated by the incoming laser signal can be represented by [28]:

$$I_{\phi} \approx G_R \eta_{\lambda} \frac{\lambda I_T}{hc} \quad (14)$$

where G_R is a gain factor dependent on the optical, material, and electrical properties of the device, η_{λ} is the quantum efficiency dependent on the light wavelength λ , h is the Planck constant, and c is the speed of light. While many device-specific factors influence G_R and make it difficult to calculate, the quantum efficiency can be approximated as unity except at wavelengths with insufficient energy to generate charge carriers within the ASIC materials. For silicon, light wavelengths longer than approximately 1100 nm are unable to excite electrons above the 1.12 eV band gap, meaning that no charge carriers can be generated.

From this model, we can see that the important factor affecting the photocurrent is the wavelength of the incident light. Longer light wavelengths will increase the generated photocurrent both by transmitting more light through the diaphragm and by having more carrier-generating photons per unit of power. This trend continues until the photons do not contain enough energy to excite charges passed the band gap (e.g., 1100 nm for silicon). At this point, the quantum efficiency and photocurrent will drop to zero.

3.5 Microphone Output Under Laser Injection

The output voltage V_{out} of the MEMS microphone can be approximated as a linear combination of the displacement of the sensing diaphragm (w) and the photocurrent generated as light interacts with the sensitive components on the ASIC (I_{ϕ}). This can be represented as

$$V_{out} \approx G_w w + G_{\phi} I_{\phi} \quad (15)$$

where G_w and G_{ϕ} are the gain factors that translate the displacement and photocurrent into voltage, respectively. These gain factors are dependent on many different properties in each MEMS microphone, and they are difficult to calculate and measure without specific knowledge of the ASIC design. Ultimately, their exact values are unnecessary in determining the cause of the output signal that we see.

The displacement of the diaphragm w can be modeled as a linear combination of the two photoacoustic effects:

$$w = w_{TE} + w_{TD} \quad (16)$$

where w_{TE} and w_{TD} are the displacement due to thermoelastic bending and thermal diffusion, respectively.

Because the output voltage is a combination of these different factors, it can be difficult to isolate and describe any one factor and its contribution to the output signal. To tackle this challenge, we design experiments to isolate and measure the contribution of each effect in the next section.

4 Experiments and Results

In this section, we present a procedure to identify the relative contributions of each of the applicable physical phenomena on the output signal of a microphone under a laser signal injection attack. In our experiments, we found that *the different designs of each microphone lead to different dominant factors being exploited in a laser signal injection attack*. With an understanding of these factors, it will be possible to make design changes to reduce the contribution of each effect, leading to MEMS microphones that are more resistant to laser signal injection. To demonstrate this procedure, we perform the characterization on eight different commercial MEMS microphones with different vendors and properties.

An overview of this procedure is shown in Fig. 3. The main idea is to isolate a single physical effect and measure the amplitude and phase response of the output signal as we sweep the modulation frequency of the input laser. We do this because the amplitude and phase responses form a way to identify each component, as each one is predicted to have a different response to the incoming light signal. Once we have a way to identify a single component, we add each of the other two components to determine their relative contribution to

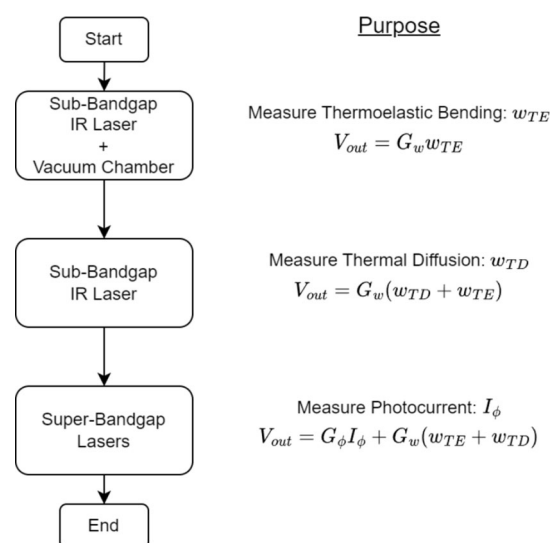


Fig. 3 The experimental procedure to determine the contributions of the three physical mechanisms to the output voltage of each microphone

the output signal. By comparing the shifts in amplitude and phase, it identifies when each component is dominant so we can obtain a characterization of the laser signal injection. The overhead to perform the procedure is relatively low as each new model of MEMS microphone only needs to be profiled once with this procedure to understand their vulnerabilities to laser injection attacks. Once the setup is developed, it only takes a few weeks for an experienced technician to carry out an in-depth study on a new device.

4.1 Experimental Setup

Here, we describe the setup used to determine the effects generated by the laser signal injection on MEMS microphones. The equipment setup we used cost less than \$10,000, with most of the cost coming from the oscilloscope and other electrical instruments which are likely already owned by MEMS microphone manufacturers.

Target Microphones

Eight different MEMS microphones were selected as targets for our experiments. These microphones are summarized in Table 1. Out of the eight targets, six of them are capacitive-sensing, while the Vesper VM1010 and VM3000 are piezoelectric-sensing microphones. Three of the microphones (ICS41350, SPH0641, and VM3000) have digital pulse density modulation (PDM) outputs, demonstrating that the laser injection affects the devices even when there is a digital output. All of the capacitive-sensing microphones have doped polysilicon diaphragms [35, 36], while the Vesper microphones have diaphragms consisting primarily of aluminum nitride [37].

The SPH0641 and the SPA1687 each have two diaphragms-backplate pairs instead of a single pair. All of the microphones except the ADMP are roughly the same package size with the same volume of air in the back cavity. The ADMP401 was included to show how a microphone is affected when there is not any light-blocking globtop, as it was the only microphone we targeted that did not have any

light protection. The ADMP also contained external amplification and filtering circuitry, but the displayed results are the signal from the microphone directly.

Signal Conditioning and Measurement

The voltage output from each of the target microphones was measured with a Stanford Research Model SR560 pre-amplifier connected to a Picoscope 5444D oscilloscope. The preamplifier was set to a low-pass filter with a 30 kHz cutoff frequency and a -6 dB/octave rolloff. All the microphones were powered with a Sigilent SPD3303C power supply set to a constant +3 V. In the case of the digital output microphones, a 0–3V 2.4MHz clock signal was generated with a Tektronix AFG3102 function generator. To convert the digital PDM signal to an analog waveform, a simple RC low-pass filter consisting of a 1 k Ω resistor and a 4.7 nF capacitor was attached to the output. A Dell XPS laptop running a custom MATLAB program with the Instrument Control Toolbox was used to obtain data from the Picoscope while simultaneously controlling the laser output with a connection to the function generator.

Controlling Optical Irradiance

In order to have precise control for our experiments, we used several tools to control the optical power and focusing of the laser output. We used five laser diodes in our experiments: a 1470 nm Mitsubishi ML920J16S, a 904 nm Thorlabs L904P010, a 638 nm Thorlabs L638P150, and a 450 nm Osram PLT5 450B. Since the optical output power of a laser diode is linearly proportional to the current across the junction, the optical power can be controlled with a variable current source. This current source was formed with a laser driver connected to a function generator. In our setup, we used a Thorlabs LDC205C laser driver, controlled by a Tektronix AFG3102 function generator. During experimentation, a Dell XPS laptop running a custom MATLAB program with the Instrument Control Toolbox was used to generate a frequency sweep on the function generator while simultaneously cap-

Table 1 The MEMS microphones used in experiments

Device	Manufacturer	Type	Output	Diaphragm	Globtop on ASIC
CMM3526	CUI Devices	Capacitive	Analog	Front	✓
SPU0410	Knowles	Capacitive	Analog	Front	✓
ICS41350	InvenSense	Capacitive	Digital	Back	✓
ADMP401	Analog Devices	Capacitive	Analog	Back	-
SPA1687	Knowles	Dual Capacitive	Analog	Front	✓
SPH0641	Knowles	Dual Capacitive	Digital	Front	✓
VM1010	Vesper	Piezoelectric	Analog	Single	✓
VM3000	Vesper	Piezoelectric	Digital	Single	✓

turing data. A Thorlabs PM100USB power meter with an S425C head was used to measure and calibrate the optical power output of the 1470 nm laser. A S121C head was used to calibrate the optical power of the rest of the laser diodes.

We developed a setup to control the aiming and focus of the laser beam using a C-mount camera, a Thorlabs LDH56-P2 laser collimation cage, two half-silvered mirrors as beamsplitters, and a Mitutoyo 5x objective lens. A Hayashi LA-100USW was used as a light source to assist in viewing the target diaphragm, but it was powered down during experimentation. In the case of the 1470 nm laser, a Thorlabs VRC2 detector card was required to aim and focus the beam. The full optical setup is shown on the both Fig. 4. This setup allowed us to visually see the focus and position of the laser beam as it was injected into the MEMS acoustic port.

Vacuum Setup

In order to test the effects of low atmospheric pressure, we performed a signal injection attack while the microphone was in a vacuum chamber. Figure 4 shows an overview of the setup. We used a BVV vacuum chamber with acrylic transparent walls and an included pressure gauge. A Zeny VP125 vacuum pump was used to evacuate air from the chamber. A Thorlabs 3-Axis manual stage with rotation was used to hold the microphone, allowing for fine control of the position and rotation of the target before turning on the vacuum. Thin copper tape was used to transport signals in and out of the vacuum chamber.

4.2 Determining the Contribution of Thermal Effects with a Sub-Bandgap IR Laser and a Vacuum Chamber

The first step in the process is to isolate a single physical phenomenon that could be generating the effects that we see

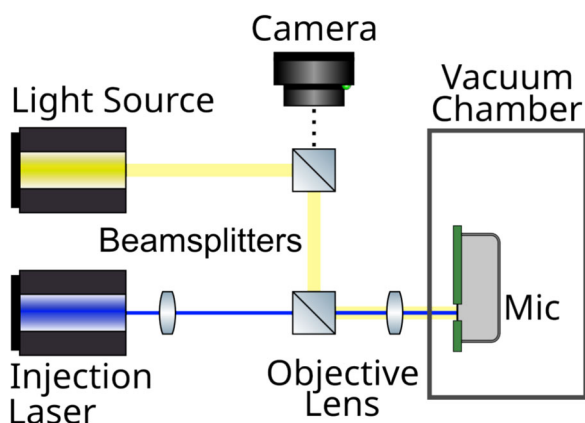


Fig. 4 Optical setup to measure microphone output while performing laser signal injection

on the output of the microphone. This effect was chosen to be the thermoelastic bending effect. This leaves two other effects to be removed: photocurrent generation and thermal diffusion.

To remove photocurrent generation, we performed a laser signal injection experiment using a 1470 nm IR laser, which has much less photon energy than the band gap of silicon. These experiments are inspired by thermal laser stimulation (TLS) failure analysis [38], where laser wavelengths longer than 1100 nm are used to generate heat but do not have enough photon energy to generate a photocurrent (see Sect. 3.4). By using a 1470 nm laser for signal injection, we ensure that thermal effects are the only phenomena generating the output signal of the microphone. While the silicon diaphragms will be fairly transparent to this wavelength of light, we found that enough energy is absorbed to have a measurable signal.

Now that we have isolated down to the thermal effects, we can differentiate between thermoelastic bending and thermal diffusion using a vacuum chamber. As mentioned in Sect. 3.3, the thermal diffusion effect is directly proportional to the ambient pressure of the air within the microphone. When we use a vacuum chamber to reduce the ambient pressure, we also reduce the contribution of the thermal diffusion effect, as there is less air to generate photoacoustic waves. When the vacuum chamber is combined with the 1470 nm laser, we can isolate the effects of thermoelastic bending alone. Once we have the thermoelastic bending component, we can determine the thermal diffusion component by repeating the experiment after reintroducing air into the vacuum chamber. The difference between the signal at low pressure and the signal at atmospheric pressure will give us the thermal diffusion component.

We performed these laser signal injection experiments on eight different commercial microphones described in Sect. 4.1 and Table 1. The laser was kept at a bias power of 5 mW and an injection signal amplitude of 1 mW. A frequency sweep of the injection laser was used to collect the amplitude and phase response of the output voltage signal. The changes in amplitude and phase provide a way to identify when each thermal component is dominant. We performed the experiment first at a pressure of 0.1 atm and then repeated the experiment at 1 atm.

The results of these experiments are presented in Fig. 5. The eight microphones are presented in eight separate subfigures. The top of each subfigure shows the amplitude response of the microphone output over the selected frequencies, while the bottom of each subfigure shows the phase response. Notice that each of the microphones had a measurable thermoelastic bending signal while under vacuum, indicating that all of the diaphragms had some innate thermal asymmetry that was being exploited by the laser signal injection. In fact, the output of the Knowles SPU0410 (Fig. 5b) seems to

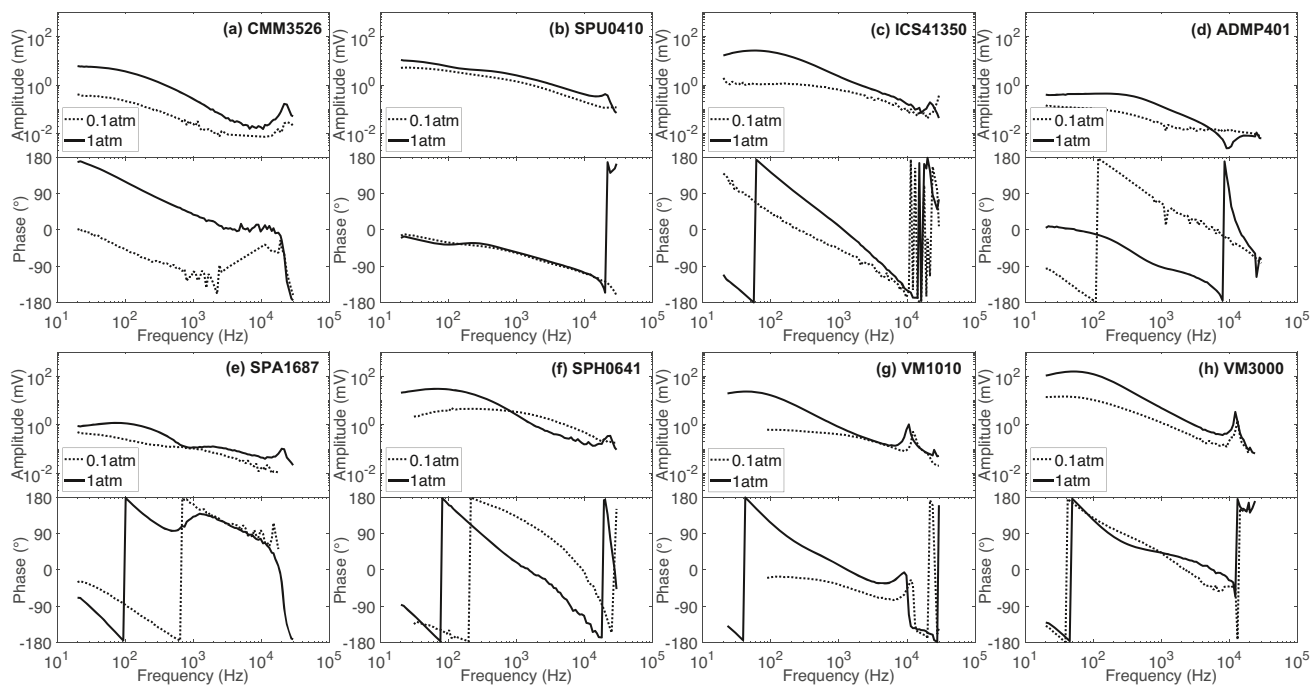


Fig. 5 The results from the vacuum chamber experiments with a sub-bandgap IR laser. All measurements were completed with a 1470 nm laser to remove photoelectric effects. The changes in the generated signal at different air pressure indicate the contribution of the ther-

be driven nearly entirely by thermoelastic bending. The rest of the microphones had significant changes to their output voltage signals as we introduced air back into the chamber, indicating the presence of thermal diffusion effects. For all of the microphones except the SPU0410, the TD component is clearly dominant over the TE component. This is demonstrated by a significant increase in output amplitude, as well as a change in the output phase, especially at low frequencies. At these low frequencies, the thermal diffusion component is out-of-phase with the thermoelastic bending component. As frequencies increase, the thermal diffusion signal gets weaker, and the output signal aligns with the thermoelastic bending signal.

4.3 A Comparison of Photoacoustic Effects and Photoelectric Effects

The next step in the process is to determine the contribution of photocurrent generation. To do this, we repeat the modulation frequency sweep experiment in Sect. 4.2 using three more wavelengths of an injection laser: a 904 nm laser, a 638 nm laser, and a 450 nm laser. All three of these wavelengths have energies above the band gap of silicon and will produce a photocurrent on sensitive parts of the ASIC circuitry. While the diaphragm will absorb these wavelengths differently and change the overall amplitude of the thermal effects, the shape

of the amplitude and phase response will remain the same. Then, any changes to the shape of the amplitude and phase response can be attributed to photoelectric generation.

The results of our experiments are shown in Fig. 6. Most of these experiments were performed with a bias power of 5 mW with a 1 mW amplitude signal. Here, we compare all three super-bandgap lasers with the sub-bandgap laser. As we can see, nearly all microphones exhibit some photoelectric effects in the ASIC. This is especially apparent when using the 904 nm laser due to its long wavelength and high diaphragm transmission, which contributes to the highest PG signal as described in Sect. 3. For most of the microphones, photocurrent generation dominates photoacoustic effects for 904 nm light. For the 450 nm laser, the trend is reversed, and the results follow very closely with the 1470 nm sub-bandgap laser. This indicates that for blue light, the signal is entirely driven by photoacoustic effects. The red 638 nm laser shows how the photoacoustic and photoelectric signals mix in many of the microphones.

To understand the characteristics of the photocurrent generation, the primary result to consider is the experiments with the 904 nm laser. Notice that the output amplitude of the PG signal is considerably higher than the photoacoustic signal for most of the microphones. Just like the photoacoustic signal, the PG signal exhibits a decrease in signal amplitude at higher frequencies. This is likely due to the electrical properties of

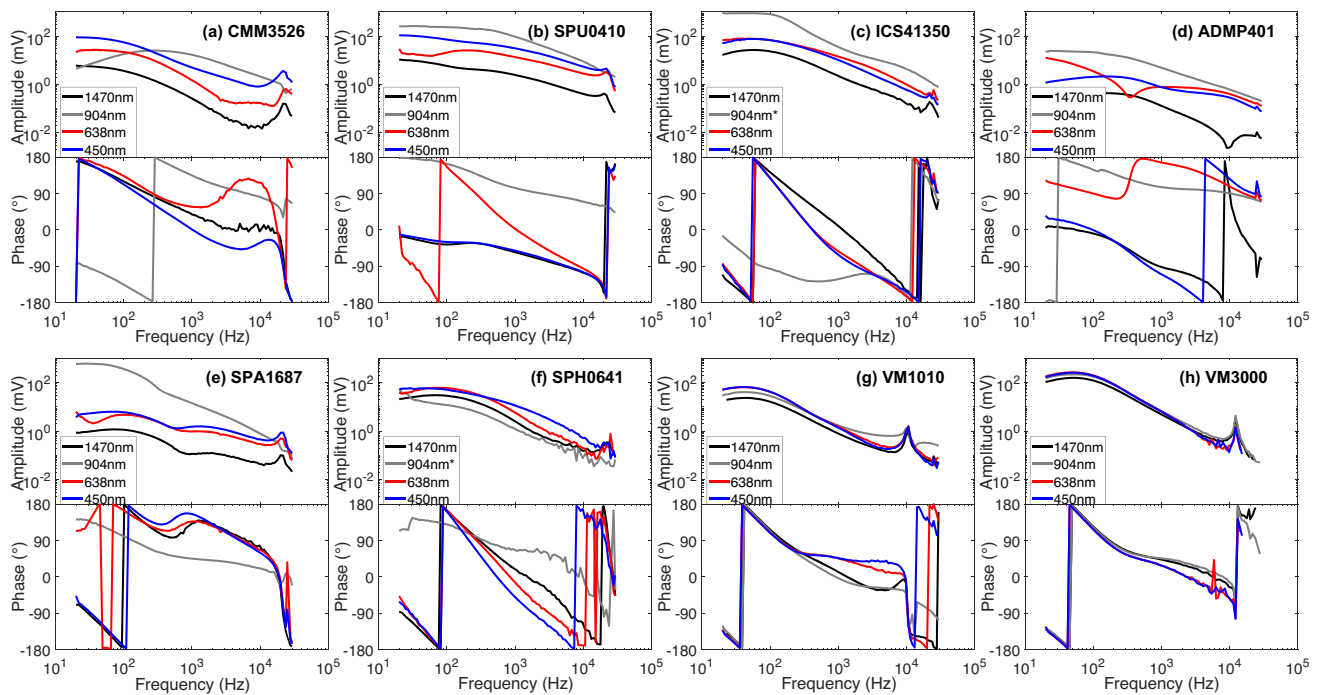


Fig. 6 A comparison of photoacoustic and photoelectric effects on MEMS microphones at 5 mW bias and a 1 mW amplitude laser signal. The effects of the 1470 nm laser are entirely due to thermal effects, while the rest will be some mixture of thermal and electric effects. (*) Asterisks indicate that the injected power was at 0.2 mW bias and 0.1 mW

the photosensitive parts of the ASIC, which are difficult to predict. From cases where the PG signal is dominant, we can see that the PG signal tends to be out-of-phase with the photoacoustic signal, leading to clear antiresonances in some of the microphones where the photoelectric and photoacoustic effects are competing for dominance. This is especially apparent for the ADMP401 (Fig. 6d), where the output from the red 638 nm laser injection has an antiresonance at 300 Hz where the PG signal is completely out-of-phase with the photoacoustic signal.

For two of the microphones, the ICS41350 (Fig. 6c) and the SPH0641 (Fig. 6f), we performed our experiments with the 904 nm laser at a reduced bias power of 0.2 mW and amplitude of 0.1 mW. We did this because the generated photocurrent was so significant that it could actually disable the output of the microphone at high enough injection power. While the exact explanation of why this occurs is difficult without a full understanding of the ASIC circuitry, we believe that it is due to the photocurrent causing a short circuit in a vital signal processing component. After the laser is turned off, the device returns to normal operation within a few seconds. This effect of temporarily disabling the microphone output with a laser has significant consequences on the security of systems using them.

amplitude to prevent disabling of the microphone. From shifts in amplitude and phase, we can see photoelectric effects dominate when the light can penetrate the diaphragm, but photoacoustic effects dominate when the light is strongly absorbed by the diaphragm

4.4 The Causality of Laser Signal Injection in Commercial Microphones

While we encourage microphone designers to determine vulnerabilities within each of their devices, we wanted to discuss the general vulnerability trends that we found during our research on these eight commercial microphones. A summary of our results is shown in Table 2. For each wavelength of incoming light, we ranked each measurable contribution of each effect from 1 (the dominant contribution) to 3 (the least contribution). This was repeated for each microphone to show how the different effects combine to produce the output voltage signal.

The primary concern in most of the microphones is the photocurrent generated on the ASIC when using superbandgap IR wavelength lasers. These longer wavelengths penetrate the diaphragms to affect the photosensitive ASIC directly. While the ASIC of almost every microphone we examined contained an opaque globtop covering for environmental protection, the globtop did not adequately protect against IR light. The two piezoelectric-sensing microphones we investigated were much more resistant to photocurrent generation, as the IR light was likely unable to penetrate the aluminum nitride diaphragm.

Table 2 A ranking of the contribution of each physical effect on the output amplitude (1=strongest, 3=weakest, an asterisk (*) denotes the microphone is temporarily disabled)

Device	IR 1470nm			IR 904nm			Red 638nm			Blue 450nm		
	TE	TD	PG	TE	TD	PG	TE	TD	PG	TE	TD	PG
CMM3526	-	1	-	-	2	1	-	1	2	-	1	-
SPU0410	1	2	-	-	-	1	1	3	2	1	3	2
ICS41350	2	1	-	2	-	1*	2	1	-	2	1	-
ADMP401	-	1	-	-	-	1	-	2	1	-	1	2
SPA1687	2	1	-	-	-	1	2	1	3	2	1	-
SPH0641	-	1	-	-	-	1*	-	1	-	-	1	-
VM1010	-	1	-	-	1	2	-	1	-	-	1	-
VM3000	-	1	-	-	1	-	-	1	-	-	1	-

The secondary concern in the microphones we investigated was the thermal diffusion photoacoustic signal. While biased towards low frequencies, the thermal diffusion signal was significantly stronger than the other photoacoustic effects in all but one of the microphones. This is especially apparent while using visible light lasers, where the majority of the incoming light is absorbed by the MEMS diaphragm. This is also the primary concern for the Vesper piezoelectric microphones, as their diaphragms absorb nearly all incoming laser signals.

Finally, several microphones exhibit a strong thermoelastic bending signal within certain frequency regions of the injected signal. This is especially apparent in the SPU0410, where the thermoelastic bending signal is the dominant photoacoustic effect at all frequency regions. For all of the other microphones, thermoelastic bending is present but often overridden by the thermal diffusion signal, especially for low frequencies.

5 Discussion

After highlighting the physical phenomena exploited in laser signal injection in MEMS microphones, we want to discuss some recommendations and considerations for preventing laser signal injection in future devices, potential vulnerabilities in other devices, and the limitations of this investigation.

5.1 Recommendations for Future Devices

With an understanding of the causality of laser signal injection into MEMS microphones, we now discuss some design recommendations to attenuate or remove the signal injection to improve the security of future devices. Some of these recommendations can be implemented at relatively low-cost by adjusting system designs or implementing changes in system software. Other countermeasures will require a redesign of the MEMS microphone, which can be costly but potentially create a more robust device. The device designers must care-

fully select the appropriate countermeasures that align with the specific requirements and cost constraints of the targeted application.

The best way to protect all future MEMS microphones is to reduce the amount of optical energy that can enter the package of the microphone. This can be done by inserting barriers that will diffract, reflect, or block the straight optical path but allow sound to travel around it. This can be done at the system level with waveguides or light-blocking meshes, but this also can be accomplished at the device level with special light-blocking structures as discussed in previous works [1]. It is important that these barriers be constructed with materials that can block light of a wide range of wavelengths, especially IR. While effective towards all laser effects, this blocking strategy often results in an inherent trade-off with acoustic sensitivity, as optical barriers are often acoustic barriers as well.

Beyond blocking light from entering the microphone entirely, the next best recommendation is to reduce the photoelectric signal. This can be done by improving the coverage and optical properties of the glob top already used in MEMS designs for environmental protection. Our investigations show that there are gaps in the protection of the glob top where a laser signal can influence sensitive junctions on the ASIC, especially with IR light. Beyond this, devices such as the Vesper piezoelectric microphones are inherently more resistant to PG effects because the MEMS structure effectively blocks nearly all incoming light. This is not the case for thin silicon structures that will be partially transparent to a wide range of super-bandgap light wavelengths.

Besides preventing photocurrent generation, it is important to build MEMS designs that are resistant to thermoelastic bending. In our experiments, we found that several of the microphones only exhibited a very small thermoelastic bending signal, while some devices such as the SPU0410 had a significantly stronger bending signal. To prevent thermoelastic bending, it is important to develop MEMS designs and processes that reduce inherent thermal stress gradients within the diaphragm. As much as possible, the diaphragms should

have symmetric thermal and mechanical properties through its thickness.

The thermal diffusion effect is probably the most challenging one to attenuate, as by its nature, microphones require the diaphragm to be in contact with the air. Tuning acoustic parameters such as increasing the volume of the back package will attenuate the signal, but it will also affect the response of the microphone. The only other ways to reduce the TD signal are to reduce the temperature of the diaphragm by reflecting optical energy away or improving thermal connections to transfer heat away from the diaphragm.

Finally, this research provides several potential mechanisms to detect laser signal injection. From a system level, it may be possible to use signal processing of the microphone signal to detect the low-frequency bias as an indication for a laser signal injection attack. Several microphones mounted on the same system can be used to check the validity of the incoming signal, potentially even using the unique phase responses to detect the presence of an attacking signal. These countermeasures have the potential to be implemented in software, protecting vulnerable devices with a low-cost update. On a device level, simple temperature sensors or light sensors can be intentionally designed into the MEMS or ASIC structure to indicate the presence of a strong light source. If the attacking signal can be detected, it can greatly improve the security of the systems using these microphones.

5.2 Hints Towards Vulnerabilities in Other Sensors

While this work breaks down the physical phenomena that lead to vulnerabilities within MEMS microphones, the phenomena that we investigated are not limited to MEMS microphones. This research provides indications of vulnerabilities in other sensors.

Any MEMS device that has an opening to allow light to enter the package is potentially vulnerable to photoelectric signal injection via laser. As MEMS structures are often designed with silicon, concentrated IR light can potentially transmit through any MEMS structure and affect ASIC circuitry. This could be a concern for any device designed to interact with an external fluid, such as MEMS ultrasonic sensors, pressure sensors, humidity sensors, or chemical sensors.

Beyond this, any sensor that uses the motion of a mechanical structure that is exposed to the environment is potentially vulnerable to photoacoustic signal injection. This includes conventional microphones, ultrasonic sensors, and pressure sensors. Our work discusses the many potential ways that this photoacoustic signal can be generated, all of which will be highly dependent on the structure and materials of the mechanical structures used in these sensors.

Finally, any sensor that uses the motion of a mechanical structure within an enclosure of air or another gas may potentially be vulnerable to photoacoustic injection via TD

effects. Thermal diffusion only requires that air within the enclosure be heated periodically, which can potentially be accomplished by heating the sensor package itself instead of any exposed MEMS structure. This would include MEMS accelerometers, gyroscopes, magnetometers, and oscillators that have movable MEMS structures within an enclosure of gas.

5.3 Model Limitations

This work seeks to investigate and model the major physical phenomena generating the laser effects on microphones. As the first work approaching this problem, it relies on certain assumptions that simplify the complex problem space and could potentially limit the model's applicability in less common conditions. Here, we iterate through these assumptions and describe the potential effects it will have on the laser signal injection on MEMS microphones.

First, we assume the MEMS diaphragm is thin ($< 10\mu\text{m}$), thermally conductive, and free to expand radially. In cases where the diaphragm is thick, thermally insular, or radially constrained, the thermoelastic bending effects can become a stronger contribution to the output signal. This is because heat cannot transfer entirely through the thickness of the diaphragm, leading to a thermal stress gradient in the diaphragm. The effect of this thermal gradient is described by Rousset's model [19] (Appendix A.2). Beyond the temperature gradient, a thick diaphragm will reduce thermal diffusion effect, as heat cannot reach the back column of air within the microphone package. Radial constraints can also lead to displacement in the transverse direction, as the diaphragm expands radially and presses against the constraints. Breaking these assumptions can lead to stronger thermal effects.

Next, we assume the laser modulation is within acoustic frequencies (0.02–20 kHz). At higher frequencies, acoustics of the microphone become a stronger factor on the microphone signal, leading to a more complex signal. This is already apparent in our experiments, as the frequencies close to 20kHz cause diaphragm structure to resonate, generating peaks in the captured signal. Beyond this, heat has less time to diffuse through the microphone, causing effects similar to the case with thick diaphragms. Higher frequencies may also lead to situations where plasmaelastic effects become a stronger contributor to the output signal. Plasmaelastic effects are caused when stress is generated in the polysilicon diaphragm due to the generation of excess charge carriers within the crystal structure (Appendix A.1). These effects tend to only be pertinent in high frequency domains, as the carrier lifetimes within a thin silicon diaphragm are expected to be very short [39, 40].

Finally, we assume that the laser injection power is low ($< 100\text{ mW}$ into the acoustic port) and that the air is transparent to the injected beam. If the beam is strongly absorbed

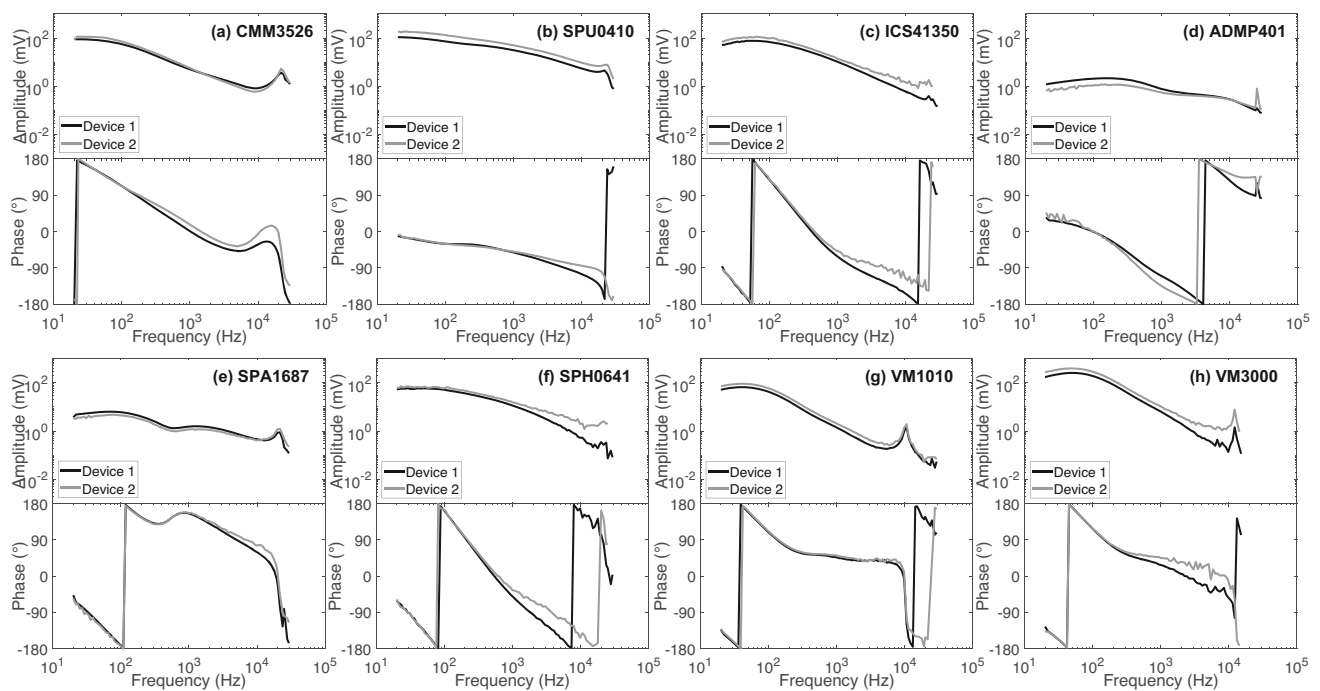


Fig. 7 A comparison between two different devices of each microphone model. All experiments were performed with a 450 nm blue laser at a 5 mW bias and 1 mW amplitude. Note the small differences in amplitude and phase, yet the frequency responses share the same trends

by the air, there are cases where a photoacoustic signal can be generated by the thermal expansion of water vapor [41] or even the direct ionization of air [42]. As laser irradiance increases, there is also the potential for ablative effects where the material is ionized and ejected from the device, generating very strong acoustic signals [43]. These effects have a high likelihood of destroying the delicate diaphragm structure.

In cases where these assumptions are broken, the laser signal injection may include other physical effects that were disregarded in this investigation, limiting the applicability of these results. Nevertheless, the assumptions of this work apply to the most common cases of low-power laser injection into existing MEMS microphone designs.

5.4 Variation Between Devices

Due to manufacturing variability, there will be slight differences between devices of the same model design. In our studies, we found that this manufacturing variability is a minor factor in comparison with the design of the microphones. To demonstrate this, we performed an experiment comparing two examples of each of the eight microphone models within this study. Each device was subjected to the same laser signal injection conditions (450 nm beam with 5 mW bias and 1 mW amplitude at atmospheric pressure), and the corresponding amplitude and phase responses were collected. The results of this experiment are shown in Fig. 7.

The results show that there are slight differences in amplitude and phase between different devices, but the output

trends of the different samples remained the same. This indicates that the design of the microphone is a much stronger factor in determining the effects of laser signal injection than any manufacturing variability. Future work may include a more thorough investigation of these small variations to provide a more thorough explanation of laser signal injection.

6 Conclusion

In this work, we presented an investigation into the physical mechanisms that enable modulated light to generate an apparent acoustic signal in MEMS microphones. We developed a model for laser signal injection into MEMS microphones and described the three primary effects of thermoelastic bending, thermal diffusion, and photocurrent generation. Using this model, we developed a procedure to isolate and measure the contribution of each physical effect to the vulnerability of the MEMS microphones. From our laser injection experiments on eight commercial MEMS microphones, we found that thermal diffusion effects provide the primary contribution for most microphones when irradiated by visible light. When irradiated by near-infrared light, photocurrent generation becomes the dominant effect in the majority of microphones. From these results, we provided recommendations to protect future MEMS microphones by improving glob top application, reducing the material asymmetries within the MEMS structure, and adding simple light or tem-

perature sensors. Finally, we discussed other sensors such as ultrasonic sensors, pressure sensors, and accelerometers that may be vulnerable to similar physical phenomena.

Appendix A

Other Physical Mechanisms

In this work, we investigated what we consider to be the most likely effects generating the effects we see in laser signal injection into MEMS microphones. But there are a few other phenomena that can potentially influence MEMS microphones. For most devices, the contribution of these effects will be very small, but can potentially become a problem for highly sensitive sensors or future microphone designs.

A.1 Plasmaelastic Bending

Within semiconductor materials, the photogeneration of electron–hole pairs will cause elastic deformations within the structure. This is due to the electrons jumping from the valence bands to the conduction bands within the semiconductor material, changing the overall charge distribution within the crystal structure. For silicon samples, the crystal structure actually contracts in response to this change in charge distribution, opposing the effects of thermal expansion. This effect was first discovered by Gauster and Habing [20], and it came to be known as the concentration-deformation mechanism [44], electronic deformation [23], or the plasmaelastic effect [29]. For many MEMS microphones, the diaphragm is made out of doped polysilicon, which can have these plasmaelastic properties.

Plasmaelastic bending is caused by a moment generated as a semiconductor changes its volume in response to the generation of charge carriers. This effect was also described in Todorović et al. [24] in a similar manner to thermoelastic bending, only with the relevant parameters related to the minority charge-carrier density instead of temperature. Similar to temperature, any generated charge carriers will diffuse almost immediately throughout the thickness of the MEMS structures. Because of this, the charge carrier generation can be approximated as uniform throughout the semiconductor portion of the MEMS structures. The excess minority charge-carrier density (Δn) in the diaphragm can be described as

$$\Delta n \approx \frac{\lambda I_A}{hcL_s(j\omega + 1/\tau)} \quad (\text{A1})$$

where L_s is the thickness of the semiconductor portion of the diaphragm, and τ is the minority carrier lifetime. The minority carrier lifetime is highly dependent on the material

properties of the semiconductor such as doping and surface recombination velocities. In general, the $1/\tau$ term will dominate the denominator of the Δn term until very high frequencies.

From here, we can predict the displacement of the diaphragm similarly to the thermoelastic effect:

$$w_{PE} = \frac{1}{4}R^2M_n\Delta n \quad (\text{A2})$$

where M_n is the moment-generating constant determined from the photoelectric properties of the materials and geometry of the diaphragm. The constant M_n is defined similarly to M_T :

$$M_n = \frac{\int_0^L d_n(z)E(z-z_n)dz}{\int_0^L E(z)(z-z_n)^2 dz} \quad (\text{A3})$$

where $d_n(z)$ is the coefficient of electronic deformation of the material at each z -coordinate.

The plasmaelastic bending was ultimately disregarded due to the likelihood of short minority lifetimes (τ) within the thin, heavily doped MEMS structures, greatly reducing the excess carrier density. Comparing thermal effects and plasmaelastic effects, previous works [39, 40] suggested that plasmaelastic effects would only be relevant at high frequencies. Beyond this, the plasmaelastic bending in silicon often causes a shift in the output phase when going from sub-bandgap to super-bandgap [45, 46]. This is because the coefficient of electronic deformation in silicon is negative and causes a contraction, which will be directly opposed to the expansion caused by the increase in temperature. We found no shift in phase in the bending signal that indicated plasmaelastic bending.

A.2 Other Thermoelastic and Plasmaelastic Bending Effects

While in Sect. 3, we discussed the effects of thermoelastic bending due to asymmetric material properties in the diaphragm, there are bending effects that can occur due to thermal and charge carrier gradients in a uniform material. These are actually the primary bending terms in most photoacoustic studies looking at thin plates [19], as previous works investigated uniform plates with thicknesses on the order of hundreds of microns. Because of these thicknesses, heat and charge carriers generated near the surface of the plate will take time to diffuse to the rest of the plate. This will lead to stress gradients and bending of the plate, with a surface-averaged quasistatic displacement of [21]:

$$w_{TB} = \frac{3R^2}{L^3}\alpha_T \int_0^L T(z)(z-z_n)dz \quad (\text{A4})$$

$$w_{PB} = \frac{3R^2}{L^3}d_n \int_0^L \Delta n(z)(z-z_n)dz \quad (\text{A5})$$

These terms were disregarded due to the thicknesses of the MEMS diaphragms being on the order of microns, and therefore the heat and charge carriers quickly diffuse through the plate. This causes the temperature and carrier concentration to be nearly uniform and reduces the bending moment to zero. If the device in question has significantly higher thicknesses or lower material diffusivity, these bending terms may become a significant contribution to the output signal.

A.3 Thermoelastic and Plasmaelastic Expansion

Beyond bending caused by stress gradients, the diaphragm will also displace due to linear expansions and contractions caused by changing temperatures and charge-carrier densities. This was first modeled by [18], showing that displacements will occur in the z -direction as the material changes size [21]:

$$w_{TX} = \frac{1}{2}L\alpha_T \int_0^L T(z)dz \quad (\text{A6})$$

$$w_{PX} = \frac{1}{2}Ld_n \int_0^L \Delta n(z)dz \quad (\text{A7})$$

In general, these terms are negligible due to the thinness of the MEMS structures.

The diaphragms will also expand radially, which can also generate a displacement in the z -direction. This effect is difficult to model as it requires specific knowledge of the mechanical boundary conditions and initial curvature of the diaphragm. In general, we do not consider this to be a strong contributor to the output signal, as MEMS diaphragms are often designed to be able to expand freely in the radial direction, but this may be a concern in some MEMS devices.

A.4 Radiation Pressure

Finally, radiation pressure will affect all the microphones under a laser signal injection attack. Radiation pressure is dependent on the light that is reflected and absorbed by the membrane, as these photons impart momentum into the membrane. Assuming the beam is normal to the plane of the membrane, the equation for the pressure imparted is

$$P_{RP} = \frac{I_A + 2I_R}{c} \quad (\text{A8})$$

where c is the speed of light. Note that the first term is due to the absorbed light, and the second term is due to the reflected light. With a quasistatic approximation, the displacement of the membrane due to this pressure is then

$$w_{RP} = \frac{A_B}{K_d} P_{RP} \quad (\text{A9})$$

For normal parameters of MEMS microphones, the displacement is on the order of a picometer per ten milliwatts

of incoming optical power, which is only measurable by extremely sensitive microphones, and it can be safely disregarded in most cases.

Acknowledgements The authors would like to thank Karl Grosh (co-founder of Vesper Technologies) for access to special equipment and illuminating conversations on the design of MEMS microphones.

Author Contributions Benjamin Cyr designed the experiments, analyzed the data, and drafted the manuscript. Vedant Sumaria and Srinivas Tadigadapa contributed to the study concept and assisted with the experiments. Yan Long and Takeshi Sugawara provided assistance with experimental design, data analysis, and manuscript editing. Kevin Fu was the principal investigator and supervisor. He reviewed the manuscript and checked it for final submission.

Funding Open access funding provided by Northeastern University Library This work was funded by Analog Devices and JSPS KAKENHI 21K11884 and 22H00519.

Data Availability MATLAB was used to collect and process the data in this manuscript. The MATLAB scripts and captured data are publicly available at <https://github.com/BenjaminCyr/MicrophoneMeasurement>.

Declarations

Conflict of Interest The authors declare no competing interests.

Ethical Approval Not applicable to this work.

Open Access This article is licensed under a Creative Commons Attribution 4.0 International License, which permits use, sharing, adaptation, distribution and reproduction in any medium or format, as long as you give appropriate credit to the original author(s) and the source, provide a link to the Creative Commons licence, and indicate if changes were made. The images or other third party material in this article are included in the article's Creative Commons licence, unless indicated otherwise in a credit line to the material. If material is not included in the article's Creative Commons licence and your intended use is not permitted by statutory regulation or exceeds the permitted use, you will need to obtain permission directly from the copyright holder. To view a copy of this licence, visit <http://creativecommons.org/licenses/by/4.0/>.

References

1. Sugawara, T., Cyr, B., Rampazzi, S., Genkin, D. & Fu, K. Light commands: laser-based audio injection attacks on voice-controllable systems. 2631–2648 (USENIX Association, 2020)
2. Ali, H., Khuttan, D., Refat, R. U. D. & Malik, H. Protecting voice-controlled devices against laser injection attacks. 1–6 (IEEE, 2023)
3. Tida, V. S. S., Shah, R. & Hei, X. in Deep learning approach for protecting voice-controllable devices from laser attacks 125–142 (IGI Global, 2022)
4. Cyr, B., Long, Y., Sugawara, T. & Fu, K. Position paper: space system threat models must account for satellite sensor spoofing. SpaceSec23, Feb (2023)
5. Xu Z, Zhang G, Ji X, Xu W (2021) Evaluation and defense of light commands attacks against voice controllable systems in smart cars. Noise & Vibration Worldwide 52:113–123

6. Chavez, C. J. et al. Systems and methods for preventing light-beam access to microphones of smart devices (2023). US Patent 11,757,531
7. Alchekov SS, Al-Absi MA, Al-Absi AA, Lee HJ (2023) Inaudible attack on AI speakers. *Electronics* 12:1928
8. Karaklajić, D., Schmidt, J. & Verbauewhede, I. Hardware designer's guide to fault attacks. *IEEE Transactions on Very Large Scale Integration (VLSI) Systems* 21, 2295–2306 (2013)
9. Dutertre, J.-M. et al. Review of fault injection mechanisms and consequences on countermeasures design. 1–6 (IEEE, 2011)
10. Yamashita, K., Cyr, B., Fu, K., Burleson, W. & Sugawara, T. Redshift: manipulating signal propagation delay via continuous-wave lasers. *IACR Transactions on Cryptographic Hardware and Embedded Systems* 463–489 (2022)
11. Park, Y., Son, Y., Shin, H., Kim, D. & Kim, Y. This ain't your dose: sensor spoofing attack on medical infusion pump (2016)
12. Shin, H., Kim, D., Kwon, Y. & Kim, Y. Fischer, W. & Homma, N. (eds) *Illusion and dazzle: adversarial optical channel exploits against lidars for automotive applications*. *Lecture Notes in Computer Science*, 445–467 (Springer International Publishing, Cham, 2017)
13. Köhler, S., Lovisotto, G., Birnbach, S., Baker, R. & Martinovic, I. They see me rollin': inherent vulnerability of the rolling shutter in CMOS image sensors (2021)
14. Yan, C., Xu, Z., Yin, Z., Ji, X. & Xu, W. Rolling colors: adversarial laser exploits against traffic light recognition. 1957–1974 (2022)
15. Bao, M.-H. *Analysis and design principles of MEMS devices* (Elsevier, Amsterdam Boston Paris [etc], 2005)
16. Manohar S, Razansky D (2016) Photoacoustics: a historical review. *Advances in Optics and Photonics* 8:586
17. Rosencwaig A, Gersho A (1976) Theory of the photoacoustic effect with solids. *J Appl Phys* 47:64–69
18. McDonald FA, Wetsel GC (1978) Generalized theory of the photoacoustic effect. *J Appl Phys* 49:2313–2322
19. Rousset G, Lepoutre F, Bertrand L (1983) Influence of thermoelastic bending on photoacoustic experiments related to measurements of thermal diffusivity of metals. *J Appl Phys* 54:2383–2391
20. Gauster WB, Habing DH (1967) Electronic volume effect in silicon. *Phys Rev Lett* 18:1058–1061
21. Todorović DM (2003) Photothermal and electronic elastic effects in microelectromechanical structures. *Rev Sci Instrum* 74:578–581
22. Todorović DM (2006) Photoacoustic elastic bending method in microelectronics – invited paper. *Journal de Physique IV (Proceedings)* 137:363–373
23. Todorović, D. M., Markushev, D. D., Rabasović, M. D., Radulović, K. T. & Jović, V. Photoacoustic elastic bending method: study of the silicon membranes. 169–172 (2012)
24. Todorović, D. M., Rabasović, M. D. & Markushev, D. D. Photoacoustic elastic bending in thin film—substrate system. *Journal of Applied Physics* 114, 213510 (2013)
25. Strahl, T., Steinebrunner, J., Weber, C., Wöllenstein, J. & Schmitt, K. Photoacoustic methane detection inside a MEMS microphone. *Photoacoustics* 29, 100428 (2023)
26. Cyr, B., Sugawara, T. & Fu, K. Why lasers inject perceived sound into MEMS microphones: indications and contraindications of photoacoustic and photoelectric effects. 1–4 (2021)
27. Shi H et al (2024) Laser-based command injection attacks on voice-controlled microphone arrays. *IACR Transactions on Cryptographic Hardware and Embedded Systems* 2024:654–676
28. Habing DH (1965) The use of lasers to simulate radiation-induced transients in semiconductor devices and circuits. *IEEE Trans Nucl Sci* 12:91–100
29. Markushev, D. D. et al. Effect of the absorption coefficient of aluminium plates on their thermoelastic bending in photoacoustic experiments. *Journal of Applied Physics* 117, 245309 (2015)
30. Soref, R. & Bennett, B. Electrooptical effects in silicon. *IEEE Journal of Quantum Electronics* 23, 123–129 (1987). <http://ieeexplore.ieee.org/document/1073206/>
31. Schinke, C. et al. Uncertainty analysis for the coefficient of band-to-band absorption of crystalline silicon. *AIP Advances* 5, 067168 (2015). Publisher: American Institute of Physics
32. Sakuragi Y, Watanabe Y, Nakamura Y, Amamoto Y (1996) Changes in optical transmittance of aluminum nitride thin films exposed to air. *MRS Proc* 449:811
33. Peña-García NN, Aguilera-Cortés LA, González-Palacios MA, Raskin J-P, Herrera-May AL (2018) Design and modeling of a MEMS dual-backplate capacitive microphone with spring-supported diaphragm for mobile device applications. *Sensors* 18:3545
34. Shubham S et al (2022) A novel MEMS capacitive microphone with semiconstrained diaphragm supported with center and peripheral backplate protrusions. *Micromachines* 13:22
35. Loeppert, P. & Lee, S. *SISONIC - the first commercialized MEMS microphone*. 27–30 (Transducer Research Foundation, Inc., Hilton Head, South Carolina, USA, 2006)
36. Weigold, J., Brosnihan, T., Bergeron, J. & Zhang, X. A MEMS condenser microphone for consumer applications. 86–89 (IEEE, Istanbul, Turkey, 2006)
37. Grosh, K. & Littrell, R. J. *Piezoelectric MEMS microphone* (2021)
38. Beaudoin, F. & Cole, E. In *Physics of laser-based failure analysis* 7 edn 196–208 (ASM International, 2019)
39. Todorovic DM et al (2015) Photoacoustic elastic bending method: characterization of thin films on silicon membranes. *Int J Thermophys* 36:1016–1028
40. Markushev, D. K. et al. Enhancement of the thermoelastic component of the photoacoustic signal of silicon membranes coated with a thin TiO₂ film. *Journal of Applied Physics* 131, 085105 (2022). Publisher: American Institute of Physics
41. Sullenberger, R. M., Kaushik, S. & Wynn, C. M. Photoacoustic communications: delivering audible signals via absorption of light by atmospheric H₂O. *Optics Letters* 44, 622 (2019). <https://www.osapublishing.org/abstract.cfm?URI=ol-44-3-622>
42. Kaleris K, Stelzner B, Hatziantoniou P, Trimis D, Mourjopoulos J (2021) Laser-sound: optoacoustic transduction from digital audio streams. *Sci Rep* 11:476
43. Shamsi, N. et al. WIP: threat modeling laser-induced acoustic interference in computer vision-assisted vehicles. *Symposium on Vehicles Security and Privacy (VehicleSec)* (2024)
44. Gusev, V. E. & Karabutov, A. A. *Laser optoacoustics*. NASA STI/Recon Technical Report A 93 (1991)
45. Datskos PG, Rajic S, Datskou I (1998) Photoinduced and thermal stress in silicon microcantilevers. *Appl Phys Lett* 73:2319–2321
46. Chenniappan V et al (2015) Characterization and modeling of photostriction in silicon cantilevers fabricated on silicon-on-insulator substrates. *J Microelectromech Syst* 24:182–191

Publisher's Note Springer Nature remains neutral with regard to jurisdictional claims in published maps and institutional affiliations.

Authors and Affiliations

Benjamin Cyr¹ · Vedant Sumaria² · Yan Long¹ · Srinivas Tadigadapa² · Takeshi Sugawara³ · Kevin Fu²

✉ Yan Long
y.long@northeastern.edu

Benjamin Cyr
bencyr@umich.edu

Vedant Sumaria
sumaria.v@northeastern.edu

Srinivas Tadigadapa
srinivas@northeastern.edu

Takeshi Sugawara
sugawara@uec.ac.jp

Kevin Fu
k.fu@northeastern.edu

¹ Computer Science and Engineering, University of Michigan,
2260 Hayward Street, Ann Arbor 48109, MI, USA

² Electrical & Computer Engineering, Northeastern University,
Dana Research Center, 100 Forsyth St, Boston 02115, MA,
USA

³ Department of Informatics, The University of
Electro-Communications, Tokyo, Japan